PERGAMON

International Journal of Heat and Mass Transfer 42 (1999) 2427–2437

International Journal of HEAT and MASS TRANSFER

Natural convection of a two-layer fluid in a side-heated cavity

A.M. Bethancourt L.[a,*], M. Hashiguchi[a], K. Kuwahara[b], J.M. Hyun[c]

[a] *Institute of Computational Fluid Dynamics, 1-22-3, Haramachi, Meguro-ku, Tokyo 152, Japan*
[b] *The Institute of Space and Astronautical Science, 3-1-1 Yoshinodai, Sagamihara, Kanagawa 229, Japan*
[c] *Department of Mechanical Engineering, Korea Advanced Institute of Science and Technology, Yusong-ku, Taejon 305-701, South Korea*

Received 6 February 1998; in final form 17 July 1998

Abstract

Comprehensive numerical computations are made of natural convection in a side-heated square cavity. Two layers of immiscible Boussinesq liquids are contained in the enclosure. Numerical solutions are acquired to the governing Navier–Stokes equations. No a priori assumptions are made on the shape and dynamical role of the interface. The behaviour of the interface is obtained as part of the solution. Attention is directed to the effect of a deformable interface and surface tension on the flow and heat transfer characteristics. Explicit influences of the capillary number and the Marangoni number are scrutinized. The global flow patterns are visualized, and local and averaged heat transfer coefficients along the wall are plotted. The limitations of the previous models using a non-deformable flat interface are pointed out.

Nomenclature

c_p specific heat at constant pressure [J kg^{-1} K^{-1}]
Ca capillary number $\mu_1 u_{ref}/\sigma_{ref}$
g acceleration of gravity [m s^{-2}]
Gr Grashof number $g\beta L^3(T_h - T_c)/\nu^2$
h dimensionless interface height
H enclosure height [m]
k thermal conductivity [W m^{-1} K^{-1}]
L enclosure length [m]
Ma Marangoni number $(\partial\sigma/\partial T)\Delta T L/(\mu\alpha)_1$
Nu local Nusselt number $-\partial\theta/\partial x$
$\overline{Nu}$ averaged Nusselt number
p dimensionless pressure $P/\rho_1 u_{ref}^2$
P pressure [Pa]
Pr Prandtl number ν/α
Ra Rayleigh number, $Gr \cdot Pr$
T temperature [K]
T_{ref} reference temperature $T_h + T_c/2$
u dimensionless velocity in x-direction U/u_{ref}
u_{ref} reference velocity $(\nu\alpha)_1^{1/2}/L\, Ra_1^{1/2}$
U velocity in x-direction [m s^{-1}]
v dimensionless velocity in y-direction V/u_{ref}
V velocity in y-direction [m s^{-1}]
x dimensionless horizontal distance X/L
X horizontal distance [m]
y dimensionless vertical distance Y/L
Y vertical distance [m].

Greek symbols

α thermal diffusivity $k/\rho c_p$
β thermal expansion coefficient [K^{-1}]
θ dimensionless temperature $T - T_{ref}/T_h - T_c$
μ dynamic viscosity [kg m^{-1} s^{-1}]
ν kinematic viscosity [m^2 s^{-1}]
ρ density [kg m^{-3}]
σ surface tension [N m^{-1}].

Subscripts

1 lower layer fluid
2 upper layer fluid
c cold
h hot
r ratio of the upper layer fluid property to the lower layer fluid property
ref reference state at T_{ref}.

* Corresponding author.

0017–9310/99/$ - see front matter
PII: S0017–9310(98)00311–1

1. Introduction

Natural convection of a Boussinesq fluid in a rectangular cavity, with its two vertical sidewalls maintained at different constant temperatures, constitutes a benchmark flow configuration. The horizontal walls are thermally insulated. Flow and heat transfer in this cavity, especially at high Rayleigh numbers and for $Pr \sim 0$ (1), have been well documented, and close agreement has been seen between numerical computations and experimental observations. The transport characteristics are of prime concern from the standpoint of fundamental research as well as in practical technological applications. Solar heat storage systems and crystal growth are salient engineering examples of the natural convection of the present problem [1–3].

The majority of the existing research has been principally devoted to the case of a single fluid filling the entire enclosure. In realistic situations, however, the fluid system oftentimes consists of two (and possibly more) separate, immiscible liquids, a layer of one liquid overlying a layer of another liquid, in the described side-heated cavity. The problem formulation now contains additional dynamical ingredients such as the interfacial stresses and the deformation of the interface shape. The behaviour of a two-layer liquid is of interest in the course of design and operation of fluid experiments in low gravity space environment [1]. Also, a multi-layered liquid arrangement provides an improved model for buoyancy-driven convection process in growing high-quality crystals [2, 3].

Sparrow et al. [4] performed a systematically-organized experiment in a square cavity using a layer of hexadecane overlying a layer of water. The physical properties of the water/hexadecane combinations are well known. By careful measurements of temperature fields, the overall heat transfer coefficient, expressed in the Nusselt number Nu, was depicted by an empirical correlation function of the properly-defined Rayleigh number and the pertinent parameters. Kimura et al. [5], by using a spindle oil–ethylene glycol combination and a spindle oil–water combination, examined the effects of the ratio of depths of two layers on the overall Nu. Parallel numerical calculations were also made by Kimura. These studies presented valuable data to gain a basic understanding of the dynamical elements involved in the natural convection of a two-layered liquid.

It is important to point out that, in the above investigations, the shape of the interface was assumed to be rigid, flat and horizontal; therefore, the vertical velocity v was taken to be zero at the interface. Also, the effect of the interfacial stresses was not taken into consideration. In the parameter spaces that were covered in the studies of Sparrow et al. [4] and Kimura et al. [5], the results obtained were consistent with the above approximations. However, the question of the applicability of the above assumptions, i.e. the effect of interface deformation and the impact of interfacial stresses, in an extended range of parameters has not been seriously addressed in the literature.

In a numerical investigation, Ramachandran [6] illustrated that the flow patterns are altered when the interfacial forces are comparable to the bouyances forces, under the assumption of a flat and rigid interface. The significance of the thermocapillary force was noted in the recent numerical study of Fontaine and Sani [7]. However, the influence of a deformable interface on the global transport phenomena was not scrutinized in detail.

In the present paper, natural convection in a square enclosure of two immiscible liquids will be formulated with no a priori assumptions on the shape and dynamical role of the interface. Knowledge on the behaviour of the interface will be gained as part of the solution, rather than as a pre-assumed flat, rigid surface separating the two liquids. The interfacial stresses are explicitly retained in the present numerical model. The key assertions of the present paper are directed to portraying the flow and thermal fields under the assumption of a deformable interface and with a proper inclusion of interfacial stresses. These imply that the present efforts are moving closer to realism; also, the present data will illuminate the usefulness and validity as well as the limitations of the preceding work.

The results of the present endeavours will be checked against the previous data which were secured under a rigid, flat interface and with no interfacial stresses included. The ranges of parameters have been widened considerably, and the averaged and local Nusselt numbers on the vertical sidewall will be displayed. For the purpose of specific comparisons, the water/hexadecane combination is adopted, and comprehensive numerical computations have been conducted.

2. Numerical method

The flow geometry and coordinate frame are sketched in Fig. 1. The fluid motions under present investigations are governed by the two-dimensional Navier–Stokes equations, with the Boussinesq fluid approximations invoked, which read, in nondimensional form:

$$\frac{\partial u}{\partial x}+\frac{\partial v}{\partial y}=0 \tag{1}$$

$$\frac{\partial u}{\partial t}+u\frac{\partial u}{\partial x}+v\frac{\partial u}{\partial y}=-\left[\lambda+\frac{1-\lambda}{\rho_r}\right]\frac{\partial p}{\partial x}+\left[\frac{\lambda+(1-\lambda)v_r}{Gr_1^{1/2}}\right]\left(\frac{\partial^2 u}{\partial x^2}+\frac{\partial^2 u}{\partial y^2}\right) \tag{2}$$

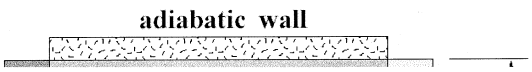

Fig. 1. Schematic of two-layered system.

$$\frac{\partial v}{\partial t}+u\frac{\partial v}{\partial x}+v\frac{\partial v}{\partial y} = -\left[\lambda+\frac{1-\lambda}{\rho_r}\right]\frac{\partial p}{\partial y}+\left[\frac{\lambda+(1-\lambda)\nu_r}{Gr_1^{1/2}}\right] \times\left(\frac{\partial^2 v}{\partial x^2}+\frac{\partial^2 v}{\partial y^2}\right)+[\lambda+(1-\lambda)\beta_r]\theta \tag{3}$$

$$\frac{\partial \theta}{\partial t}+u\frac{\partial \theta}{\partial x}+v\frac{\partial \theta}{\partial y}=\left[\frac{\lambda+(1-\lambda)\alpha_r}{Pr_1 Gr_1^{1/2}}\right]\left(\frac{\partial^2\theta}{\partial x^2}+\frac{\partial^2\theta}{\partial y^2}\right). \tag{4}$$

The symbol λ is used to control the properties in the two layers.

$$\lambda=\begin{cases}1 & \text{in the lower layer} \quad \text{(fluid 1)}\\ 0 & \text{in the upper layer} \quad \text{(fluid 2)}\end{cases}.$$

In the present calculations, the ratios of physical properties of the liquids have been selected as $\rho_r = 0.7754$, $\beta_r = 3.2470$, $k_r = 0.2407$, $\mu_r = 3.5214$, $\nu_r = 4.5413$, $\alpha_r = 0.7858$, in order to simulate the experimental particulars of the water–hexadecane combination of Sparrow et al. [4] and Ramachandran [6].

Initially, a two-layer system of immiscible fluids at equal heights ($H_1 = H_2 = 0.5\,H$) fills a square cavity of height H. They are at rest and under the condition of uniform temperature ($\theta = 0$). Suddenly, at dimensionless time $t = 0$, a differential heating is applied at the vertical walls, and the horizontal walls are thermally insulated. The associated boundary conditions at the solid wall are stipulated:

$$\text{at } x=0; \quad \theta = 0.5, \quad u = v = 0$$

$$\text{at } x=1; \quad \theta = -0.5, \quad u = v = 0$$

$$\text{at } y=0,1; \quad \frac{\partial\theta}{\partial y}=0, \quad u = v = 0.$$

At the interface, the location and shape of which are to be determined, physical considerations lead to [1]:

$$\mu_r\left\{2\frac{\partial h}{\partial x}\left[\frac{\partial v}{\partial y}-\frac{\partial u}{\partial x}\right]+\left[1-\left(\frac{\partial h}{\partial x}\right)^2\right]\left(\frac{\partial u}{\partial y}+\frac{\partial v}{\partial x}\right)\right\}_2 -\left\{2\frac{\partial h}{\partial x}\left[\frac{\partial v}{\partial y}-\frac{\partial u}{\partial x}\right]+\left[1-\left(\frac{\partial h}{\partial x}\right)^2\right]\left(\frac{\partial u}{\partial y}+\frac{\partial v}{\partial x}\right)\right\}_1 =\left[\frac{Ma}{Pr_1 Gr_1^{1/2}}\right]\left[\frac{\partial\theta}{\partial x}+\frac{\partial h}{\partial x}\frac{\partial\theta}{\partial y}\right]G_2^1 \tag{5}$$

$$\left[\frac{1}{CaGr_1^{1/2}}+\frac{Ma}{Ra_1}\theta\right]G^{-\frac{3}{2}}\frac{\partial^2 h}{\partial x^2} -\frac{2}{Gr_1^{1/2}}G^{-1}\left\{\left[\frac{\partial u}{\partial y}+\frac{\partial v}{\partial x}\right]_1-\mu_r\left[\frac{\partial u}{\partial y}+\frac{\partial v}{\partial x}\right]_2\right\}\frac{\partial h}{\partial x} =-(p_1-p_2)+\frac{2}{Gr_1^{1/2}}G^{-1}\left\{\left[\left(\frac{\partial h}{\partial x}\right)^2\frac{\partial u}{\partial x}+\frac{\partial v}{\partial y}\right]_1 -\mu_r\left[\left(\frac{\partial h}{\partial x}\right)^2\frac{\partial u}{\partial x}+\frac{\partial v}{\partial y}\right]_2\right\} \tag{6}$$

$$\left[\frac{\partial\theta}{\partial y}-\frac{\partial h}{\partial x}\frac{\partial\theta}{\partial x}\right]_1=k_r\left[\frac{\partial\theta}{\partial y}-\frac{\partial h}{\partial x}\frac{\partial\theta}{\partial x}\right]_2 \tag{7}$$

where $G = [1+(\partial h/\partial x)^2]$. In addition, the kinematic condition must be satisfied at the interface ($u_1\cdot\hat{n}_i = u_2\cdot\hat{n}_i = 0$), meaning that there is no net mass flux through the interface.

The numerical solution procedure of the present work is largely based on the PISO algorithm [8]. Space derivatives are discretized by means of second-order central differencing schemes, except the convective terms for which the third-order upwind schemes are utilized [9]. The steady-state features are of major interest, however, time-marching integrations using the Euler method, are carried out. Convergence was declared when the residual of governing equations was less than 10^{-3}. In an effort to obtain a higher resolution near the solid walls and the interface, coordinate transformations are introduced to cluster the grid points in the regions of large flow gradients. To this end, an algebraic stretching function has been adopted [10].

$$\eta=\zeta+(1-\zeta)\cdot\frac{\ln\left\{\left\{\phi+\left[\frac{(2\zeta+1)y}{H}\right]-2\zeta\right\}\Big/\left\{\phi-\left[\frac{(2\zeta+1)y}{H}\right]+2\zeta\right\}\right\}}{\ln[(\phi+1)/(\phi-1)]} \tag{8}$$

in which ϕ is an adjustable clustering parameter, and ζ indicates the location of clustering. Systematic evaluations were made to establish grid-convergence of the numerical results. For the present test cases, grid meshes of 33×33, 49×49, 65×65 and 80×80 were deployed, and an evaluation of the flow and thermal fields as well as the specific values of the averaged Nusselt number

showed no significant departures when increasing the mesh from 65×65 to 80×80, i.e. the computed output of the averaged Nusselt number, for the high Ra case, differed less than 3% from each other. Therefore, for the present calculations, the 65×65 grid is utilized.

3. Results and discussion

As stated previously, the two-dimensional flow assumption is invoked in the present work. Obviously, this is the first step toward obtaining a rudimentary understanding of the major dynamical elements involved. In a realistic three-dimensional situation, some of the flows portrayed under the two-dimensional assumption, in particular, the complex time-dependent flow patterns, may not be fully reproduced. However, knowledge of the idealized two-dimensional flows constitutes an essential building block to explore more complicated three-dimensional flows, and this is the intent of the present effort. Steps are being taken for the computation of three-dimensional flows, and they will be reported in forthcoming papers.

Two groups of computations (Table 1), Case 1 for $Ra_1 = 4.9 \times 10^5$ and Case 2 for $Ra_1 = 2.63 \times 10^7$, are designed to demonstrate how the flow and thermal characteristics are altered by the afore-stated two dynamic factors: (1) the deformation of the interface and (2) the interfacial stresses.

The general flow features of a two-layered convection are captured in Fig. 2 for Case 2a, for which the interface is assumed to be flat and non-deformable. Each layer is occupied by a clockwise circulating cell, and a weak counterclockwise cell is seen in the lower-layer-side of the interface. The isotherms are crowded near the vertical sidewalls, and in much of the interior core, the isotherms are largely horizontal. Strong temperature gradients are discernible in the vicinity of the interface. In order to satisfy the overall balance of vertical heat fluxes, the isotherms are highly skewed near the interface, and a jump in the temperature gradient is seen across the flat interface.

Figure 3 displays the results of Case 2b, in which the interface is allowed to deform, but the Marangoni convection is absent ($Ma = 0$). The value of the capillary number was set to $Ca = 5.7 \times 10^{-4}$, which closely reflects the realistic conditions attainable by the water–hexadecane combination in the experiment of Sparrow et al. [4]. For this specific parameter set, the deviations in global flow structure from Case 2a are seen to be insignificant. The present data are, therefore, supportive of the assumption of a flat, rigid interface which was invoked by Sparrow et al. [4] to deal with the particular set of water–hexadecane combination used in their experiment.

Now, the explicit influence of interfacial stress is scrutinized. For the above realistic water–hexadecane combination, the dependence of σ on T can be estimated $(\partial\sigma/\partial T)_{\mathrm{ref}} = -0.0909$ dynes cm^{-1} K^{-1}. This gives $Ma \cong 2.9 \times 10^5$ [11], leading to Case 2c with $Ca = 5.7 \times 10^{-4}$, the flow features of which are depicted in Fig. 4. Even for this parameter set, the general globalized patterns demonstrate relatively minor departures from those of the case of a rigid, flat interface of Case 2a. However, as will be asserted later, the localized behavior near the interface, in particular, in the vicinities of sidewalls, is markedly altered by the inclusion of the interface deformation and of the interfacial stresses.

Figure 5 exhibits the profile of deformable interface, as computed in the present endeavours. The vertical location of interface is highest near the hot sidewall, and the height of interface decreases smoothly as it moves toward the cold sidewall. Approximately near the center line of the cavity, the height of interface is closer to the undisturbed level, $y = 0.5$. For the present parameter ranges which are pertinent to realistic water–hexadecane combinations, the maximum deformation of interface is relatively small, reaching about 2% of the original interface height. However, as mentioned previously, the interface deformation could become appreciable as the capillary number takes large values.

The impact of Marangoni convection is discernible in several points. First, due to the presence of interfacial stress, the entire flow field tends to be invigorated. The strengthening of the flow is pronounced in the plot of

Table 1
Exemplary cases of computed results

			Deformable interface	
		Flat interface ($Ca = 0$)	$Ca = 5.7 \times 10^{-4}$	$Ca = 5.75 \times 10^{-3}$
$Ra_1 = 4.9 \times 10^5$	$Ma = 0$	Case 1a	Case 1b	—
	$Ma = 1.6 \times 10^5$	Case 1c	Case 1d	Case 1f
$Ra_1 = 2.63 \times 10^7$	$Ma = 0$	Case 2a	Case 2b	—
	$Ma = 2.9 \times 10^5$	—	Case 2c	—

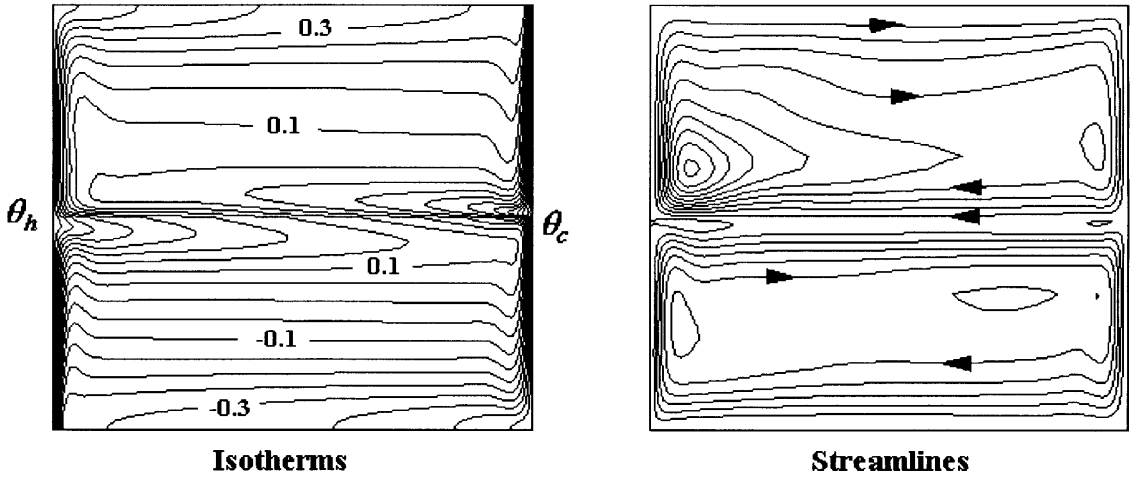

Fig. 2. Flow and thermal fields for Case 2a: $Ra_1 = 2.63 \times 10^7$, $Ma = 0$ and $Ca = 0$.

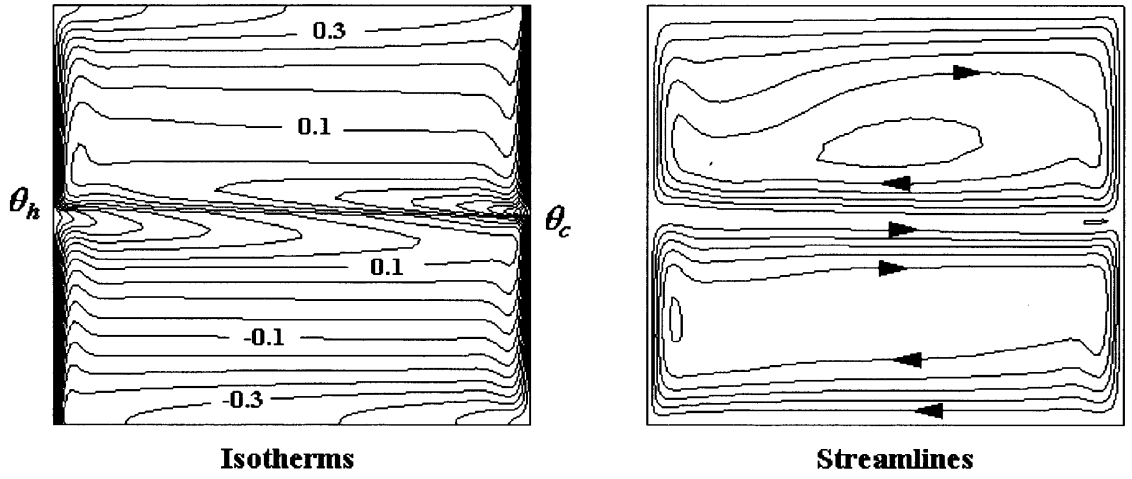

Fig. 3. Flow and thermal fields for Case 2b: $Ra_1 = 2.63 \times 10^7$, $Ma = 0$ and $Ca = 5.7 \times 10^{-4}$.

the velocity components along the interface, which is illustrated in Fig. 6. Note that the relative influence of Marangoni convection is appreciable for Case 1, $Ma/Ra \sim 0$ (1), as opposed to Case 2 for which $Ma/Ra \sim 0$ (10^{-2}).

Further evidence of the above-mentioned assertion is given in Figs 7–10, in which the flow pattern for Case 1 is plotted. In the absence of surface tension induced stresses ($Ma = 0$, for Cases 1a and 1b), as seen in Figs 7 and 8, the flow features are very similar. This suggests that interface deformation has negligible influence on the processes taking place within the cavity. When compared with Case 2, the isotherms of Case 1 are less crowded along the vertical sidewalls, indicating a thicker boundary layer. The distortions of isotherms are generally more pronounced, which is reflective of stronger convective activities within the enclosure.

In each layer, a clockwise circulating cell of almost equal strength is present, with a weak counterclockwise cell appearing in a thin area beneath the interface. In fact, it is observed that the interactions of convective processes between the two layers are reduced to this thin area, and in other regions of the enclosure, they seem to proceed independently of each other.

As shown in Figs 9 and 10, inclusion of the Marangoni convection ($Ma = 1.6 \times 10^5$, Cases 1c and 1d) results in a strong coupling between the processes in both layers. The described patterns are completely changed, and the overall flow is invigorated by the presence of surface tension effects ($Ma/Ra \sim 0$ (1)). First, it is worth pointing

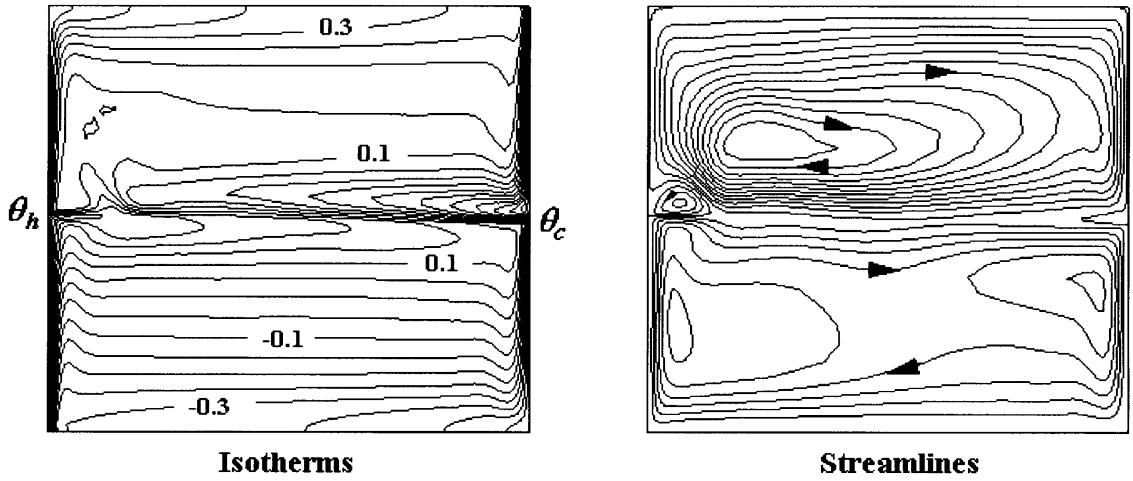

Fig. 4. Flow and thermal fields for Case 2c: $Ra_1 = 2.63 \times 10^7$, $Ma = 2.9 \times 10^5$ and $Ca = 5.7 \times 10^{-4}$.

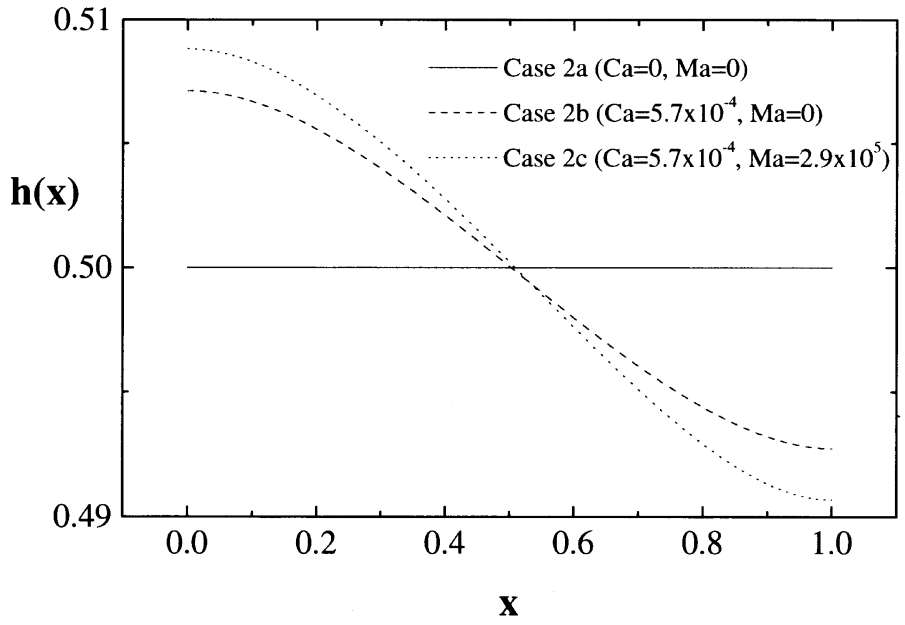

Fig. 5. Interface deformation for Cases 2a, b and c.

that no strictly steady state is achieved. Instead, a periodic flow pattern is observed after an initial transition stage is passed. A pair of vortices are observed to be ejected periodically near the interface in the vicinity of the hot wall. This ejection appears to coincide with the release of a thermal plume-like feature in the flow visualizations. The isotherms near the interface recede back and forth between the hot and cold walls, which produce the ejection of the plume after the meeting of the hot and cold fronts takes place. An enlarged description of the detailed examinations of the oscillatory behaviour will be given in a separate paper. Now, a single clockwise circulating cell is visible in the lower layer and because of the added contribution of the Marangoni force, the previously observed weak counterclockwise circulation cell vanishes in the bottom layer. Two strong counterclockwise cells appear on the upper part of the interface close to the sidewalls in addition to a weaker one at the center of the cavity; they are caused by strong velocity gradients that occur near the interface, as shown in Fig. 6. The previously reported sole clockwise circulating cell has now been displaced to the upper half part of the upper layer.

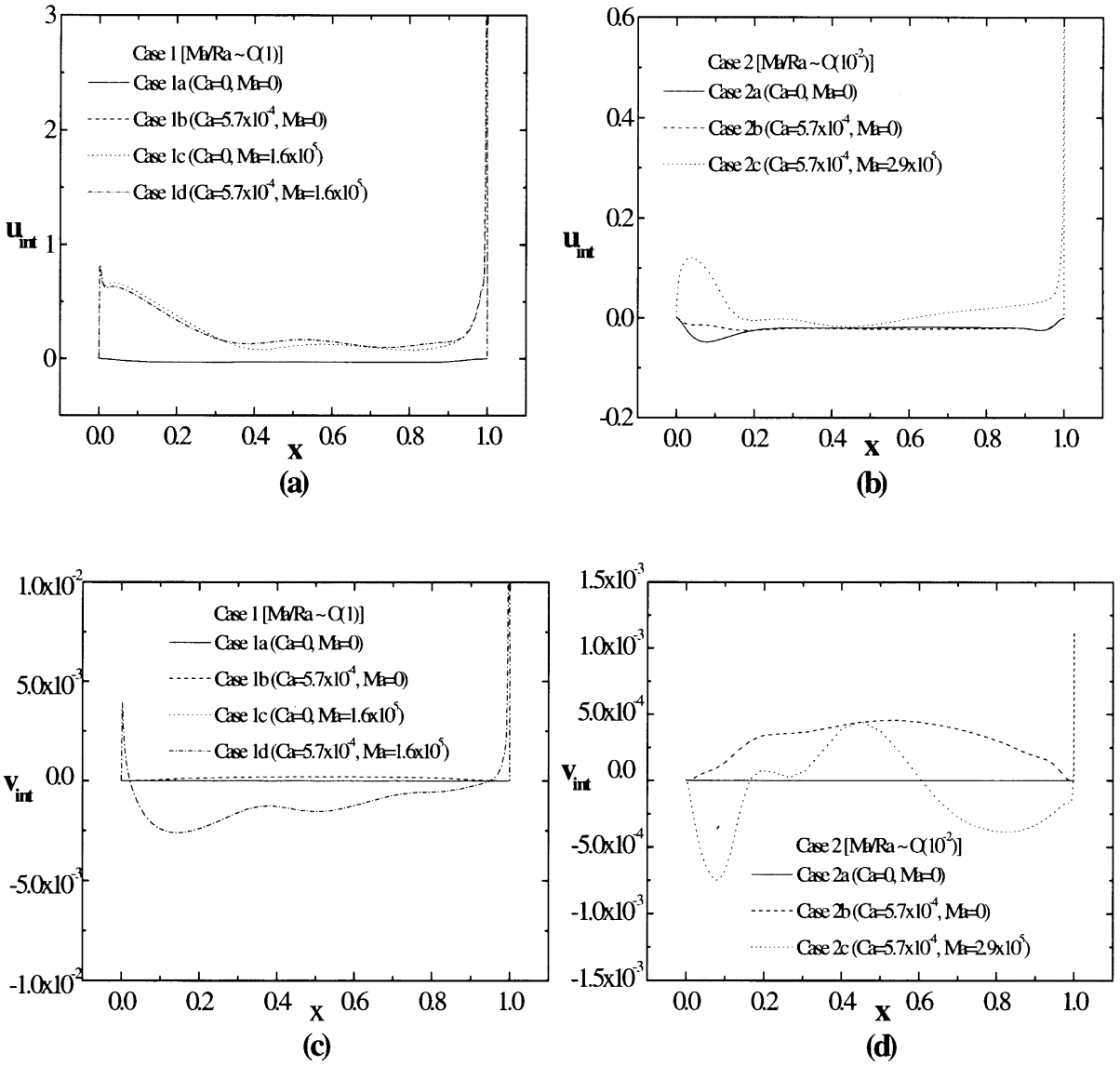

Fig. 6. Velocity distribution along the interface: (a) and (b) horizontal component; (c) and (d) vertical component.

The isotherms are greatly distorted along the interface in which steep gradients are seen. Due to the steep gradients in velocity, they are packed at the cold end of the interface and spread from the hot end. This suggests the locations for maximal heat transfer along the sidewalls.

Again, the deformation of interface is found to be negligible for the parameter set of the present computations, as shown in Fig. 11. Its maximum deformation is less than 0.4% of the initial configuration based on a flat, horizontal interface shape. This supports the reasonableness of the assumption of a flat, rigid interface invoked in a previous study [6].

3.1. Heat transfer

The effect of surface tension on the behaviour of local heat transfer coefficient is shown in Fig. 12. For the present parameter values, as pointed out earlier, the interface deformation is negligible, and this trend is more pronounced as Ra decreases. However, the local behaviour of Nu is greatly altered by inclusion of surface tension effect.

When $Ma/Ra \sim 0$ (1), for Cases 1c and d, sharp gradients are observed at both sidewall ends around the heights of the interface. At the hot wall, a substantial increase

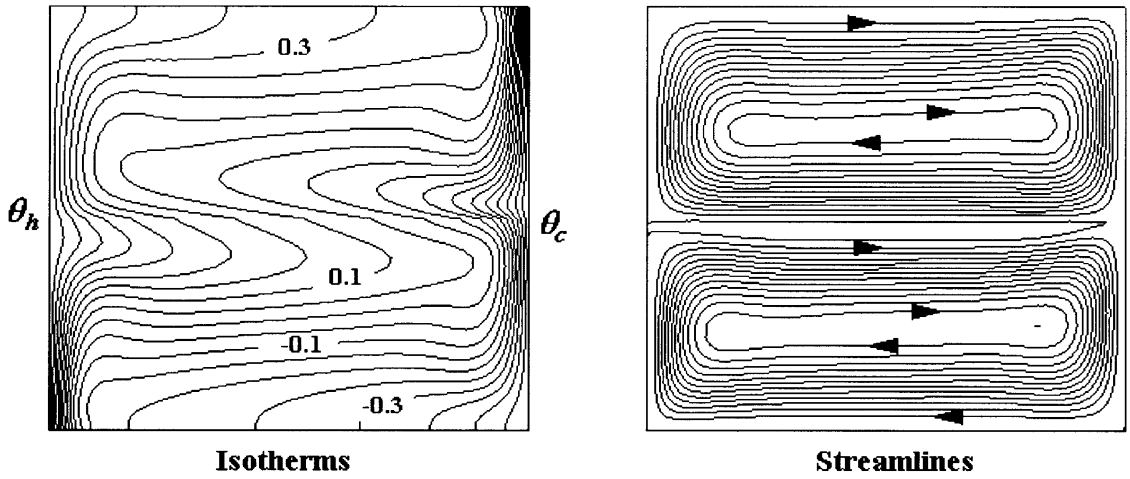

Fig. 7. Flow and thermal fields for Case 1a: $Ra_1 = 4.9 \times 10^5$, $Ma = 0$ and $Ca = 0$.

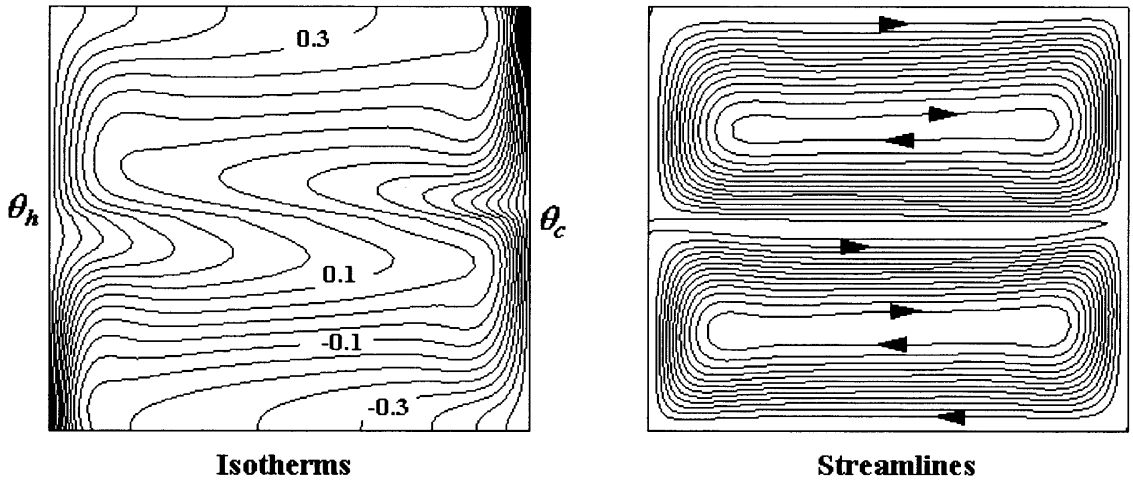

Fig. 8. Flow and thermal fields for Case 1b: $Ra_1 = 4.9 \times 10^5$, $Ma = 0$ and $Ca = 5.7 \times 10^{-4}$.

occurs over the whole length of the wall. Locally, a double peak appears near the interface regions in which a strong counterclockwise circulation cell above the interface interacts with an equally strong clockwise cell in the lower layer, as seen in Figs 9 and 10. At the cold wall, as a jet-like induced flow impinges the wall, heat transfer is greatly enhanced around the interface location; however, locally, the coefficient of heat transfer decreases on the upper side of the wall, and it remains almost unchanged when compared with Cases 1a and b. When $Ma/Ra \sim 0$ (10^{-2}), for Case 2c, since buoyancy is still the dominant cause convection, changes are appreciable locally. The double peak is absent as the strength of surface tension diminishes. At the cold wall, similar profiles are obtained along the wall except for a dramatic increase in a small region around the interface. This result seems to suggest that, as the thickness of thermal boundary layer decreases (high Ra number), the effects of surface tension on the heat transfer coefficients are confined to a small region around the interface.

4. Conclusions

Extensive numerical computations have been performed under the assumption of a deformable interface and with the inclusion of surface tension effects. The results of the preceding studies using a flat, non-deformable interface are found to be qualitatively valid for those specific ranges of parameters concerned. The present model results indicate that the interface deformation can be appreciable when the capillary number is large.

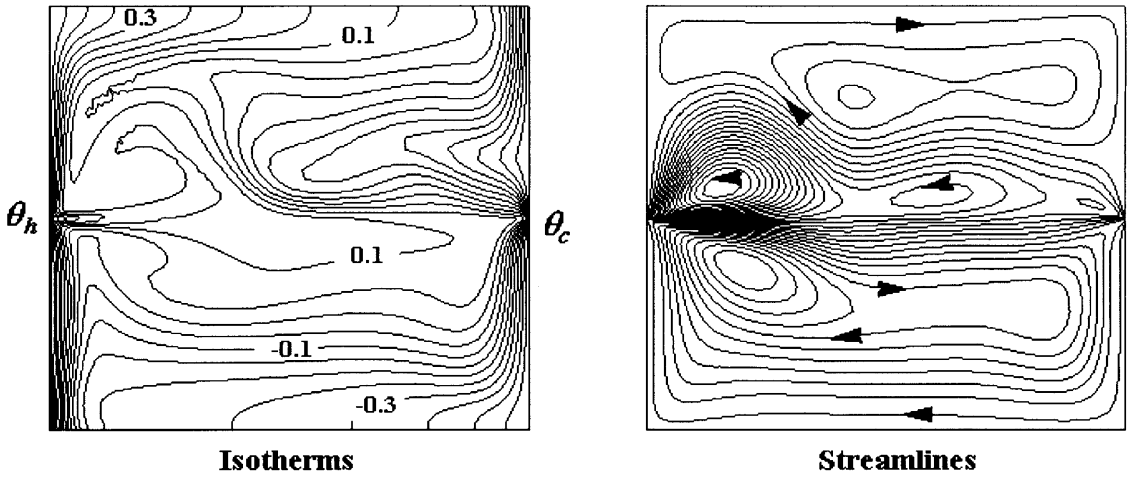

Fig. 9. Flow and thermal fields for Case 1c: $Ra_1 = 4.9 \times 10^5$, $Ma = 1.6 \times 10^5$ and $Ca = 0$.

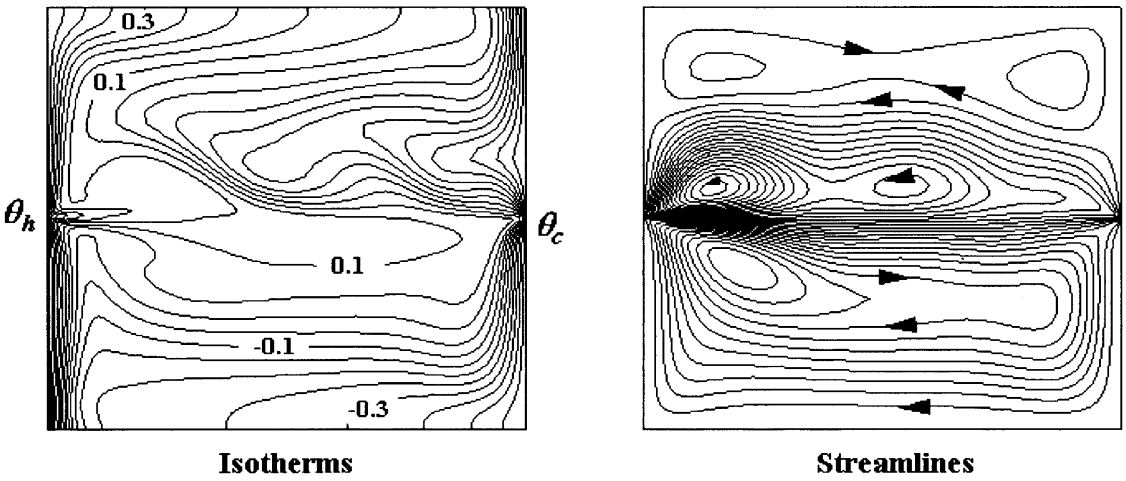

Fig. 10. Flow and thermal fields for Case 1d: $Ra_1 = 4.9 \times 10^5$, $Ma = 1.6 \times 10^5$ and $Ca = 5.7 \times 10^{-4}$.

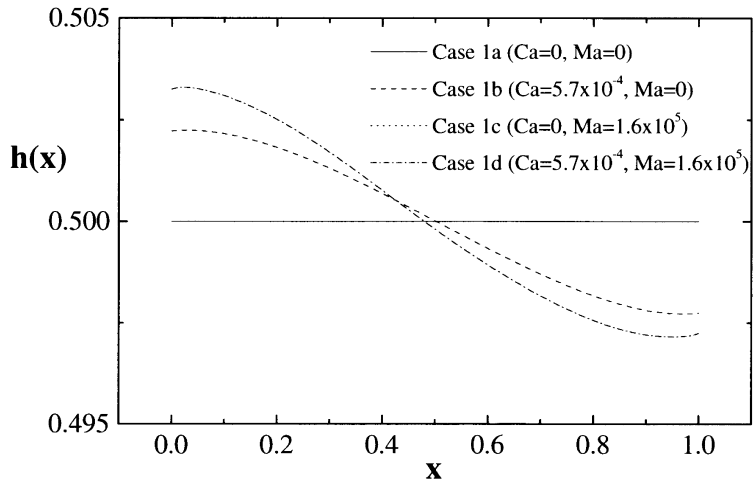

Fig. 11. Interface deformation for Cases 1a, b, c and d.

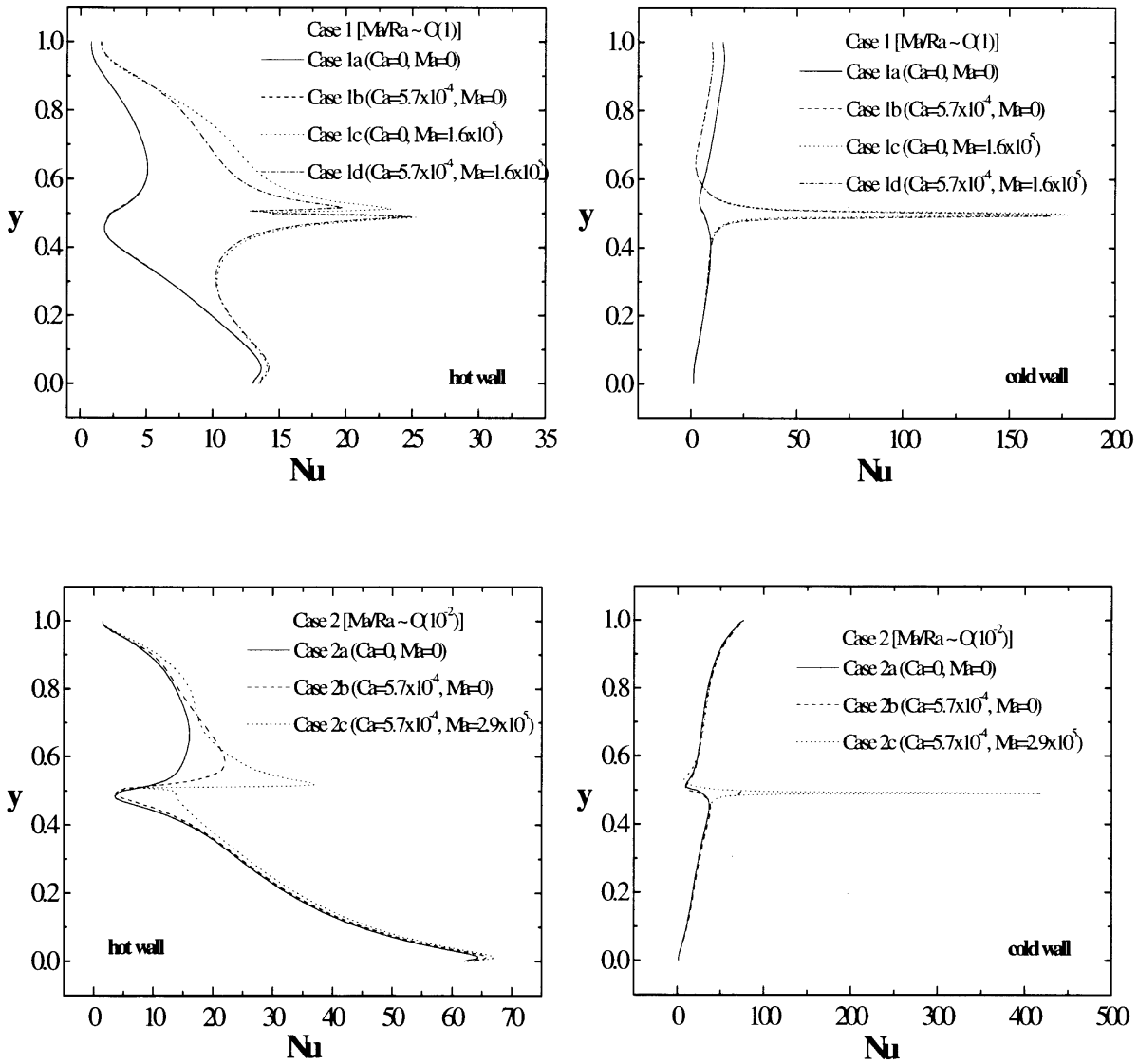

Fig. 12. Distribution of local heat transfer coefficient along sidewalls.

Qualitative changes are seen in the overall flow patterns when *Ca* and *Ma* take large values. This trend becomes more conspicuous in the velocity and temperature fields in the vicinities of sidewalls and interface. Localized flow invigoration is seen near the interface when the surface tension effect is substantial.

The impacts of a deformable interface and of surface tension are notable in local behaviour of heat transfer characteristics. Local heat transfer enhancement at side walls is evident near the region of interface when the explicit role of surface tension is included.

References

[1] S. Ostrach, Low-gravity fluid flows, Ann. Rev. Fluid Mech. 14 (1982) 313–345.
[2] W.E. Langlois, Buoyancy-driven flows in crystal-growth melts, Ann. Rev. Fluid Mech. 17 (1985) 191–215.
[3] D. Schwabe, Surface-tension-driven flow in crystal growth metals, Crystal 11 (1986) 848.
[4] E.M. Sparrow, L.F.A. Azevedo, A.T. Prata, Two-fluid and single-fluid natural convection heat transfer in an enclosure, ASME J. Heat Transfer 108 (1986) 848–852.
[5] T. Kimura, N. Heya, M. Takeuchi, H. Isomi, Natural con-

vection heat transfer phenomena in an enclosure filled with two stratify fluids. JSME (B) 52 (1986) 617–625 (in Japanese).

[6] N. Ramachandran, Thermal buoyancy and Marangoni convection in a two fluid layered system—a numerical study, AIAA 28th Aerospace Science Meeting, Reno, Nevada, 1990.

[7] J.-P. Fontaine, R.L. Sani, Flow and transport in a multi-layered fluid system—I: influence of 1- or μ-g environment, Int. J. Heat Mass Transfer 39 (1996) 2751–2770.

[8] R.I. Issa, Solution of the implicitly discretised fluid flow equations by operator-splitting, J. Comput. Phys. 62 (1985) 40–65.

[9] T. Kuwamura, K. Kuwahara, Computation of high Reynolds number flows around a circular cylinder with surface roughness, AIAA paper 84-0340, 1984.

[10] K.A. Hoffmann, Computational Fluid Dynamics for Engineers, Engineering Education System, Austin, TX, 1989.

[11] N.B. Vargaftik, Tables on Thermophysical Properties of Liquids and Gases, Hemisphere, Washington, DC, 1975.